

Supplementary Materials: The following are available online at www.mdpi.com/xxx/s1, Figure S1: spatial and temporal baseline plot of 34 Envisat SAR acquisitions for the descending track 18 covering the eastern part of the Haiyuan fault, Figure S2: 3D and planar geometry for InSAR observation, Figure S3: comparison of wet delay maps from MERIS and ECMWF for 4 largely cloud-free acquisitions, Figure S4: the results for the regional discretization, Figure S5: the fine horizontal velocity field inverted jointly by InSAR and GPS for the northeastern margin of the Tibetan Plateau. Figure S6: Regional seismicity map with 19 moderate earthquake since 1986, and Figure S7: The GPS velocity field from Gan et al. [22] for the northeastern margin of the Tibetan Plateau.

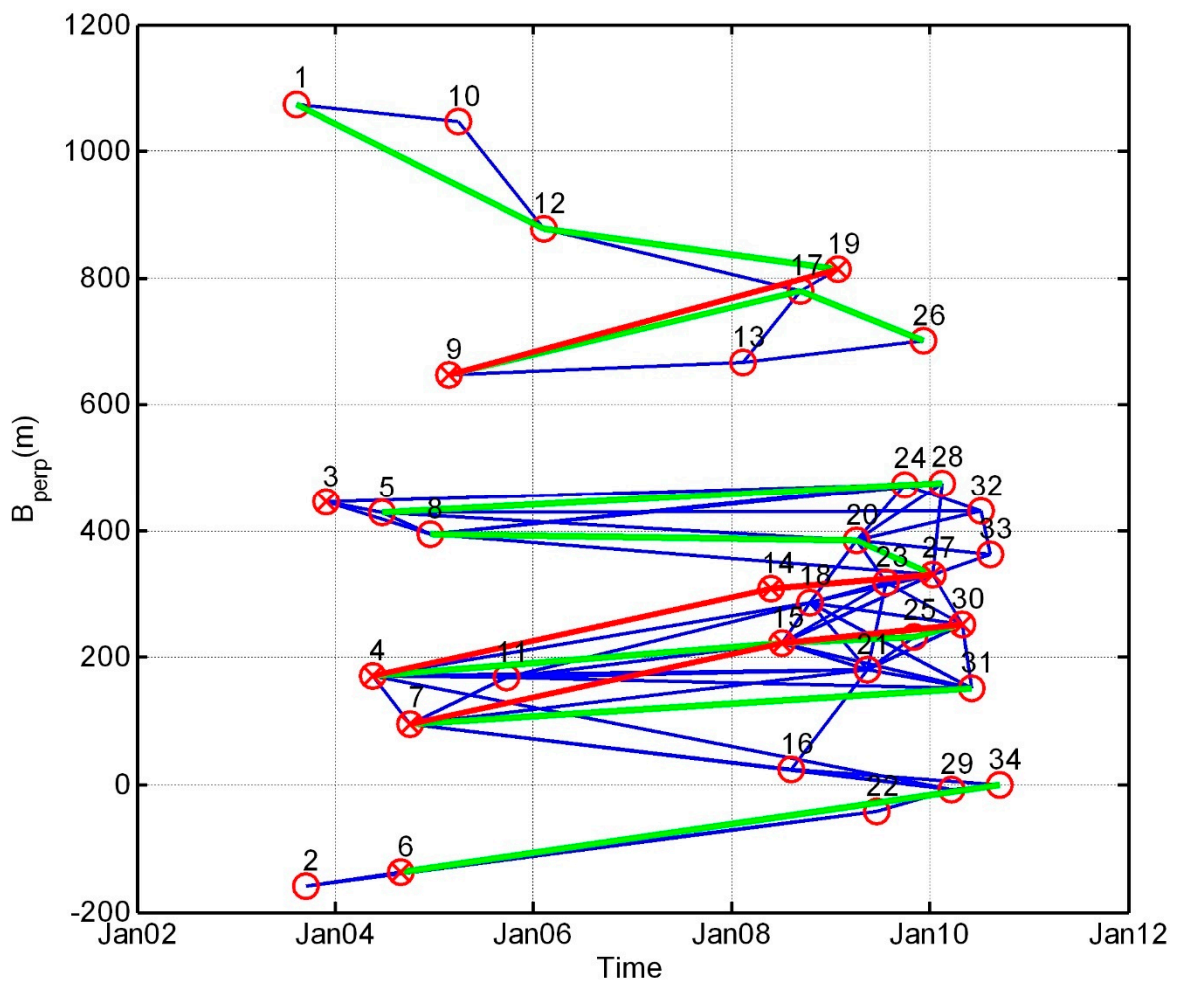


Figure S1. Spatial and temporal baseline plot of 34 Envisat SAR acquisitions for the descending track 18 covering the eastern part of the Haiyuan fault. Acquisitions span a seven year period from 2003–2010. Acquisitions are numbered time sequentially, and 10 of them marked with a red cross are largely cloud-free; The 3 interferogram chains marked by red lines were corrected for atmospheric effects using MERIS data, and 7 interferogram chains marked by green lines were corrected by using ECMWF data.

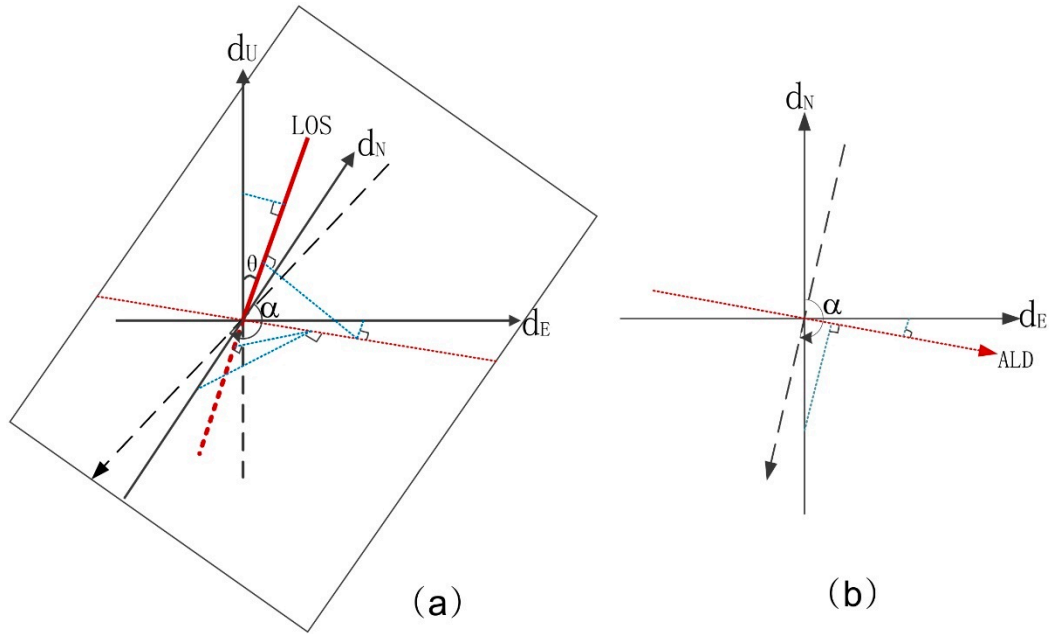


Figure S2. 3D and planar geometry for InSAR observation. (a) 3D geometry sketch map for InSAR observation. LOS is the line of sight, d_U is the vertical deformation component, d_N is N-S deformation component, d_E is the E-W deformation component, α is the heading of SAR satellite, and θ is the incidence angle. (b) Planar projection for (a). ALD is the azimuth look direction, i.e. the planer projection of LOS.

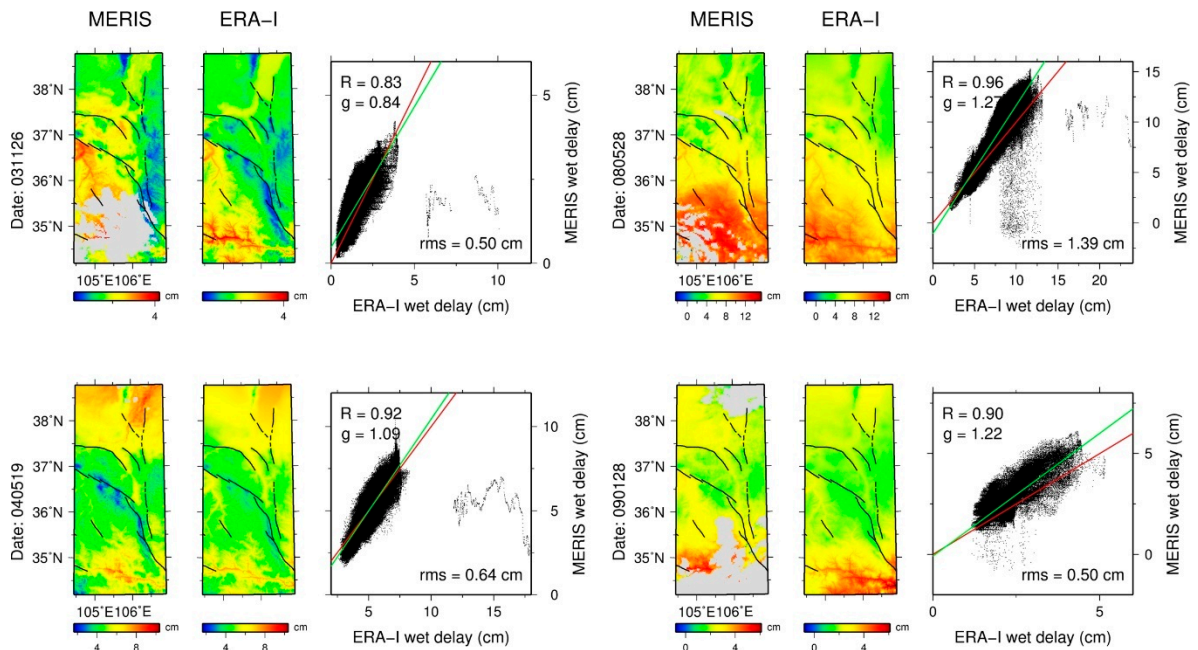


Figure S3. Comparison of wet delay maps from MERIS and ERA-I (the ERA-Interim reanalysis model, hereafter called ERA-I, is a global atmospheric model computed by the ECMWF) for 4 largely cloud-free acquisitions. Each panel displays (left column) the MERIS-derived wet

delay, (middle column) the ECMWF-derived wet delay, and (right column) scatter plot of individual pixels from MERIS and ECMWF wet delay maps. R is correlation coefficient of the best fitting line shown in green, g its gradient, and rms is the RMS misfit between the two datasets. The red line is 1:1 correspondence. All the acquisitions show a good correlation between these two datasets.

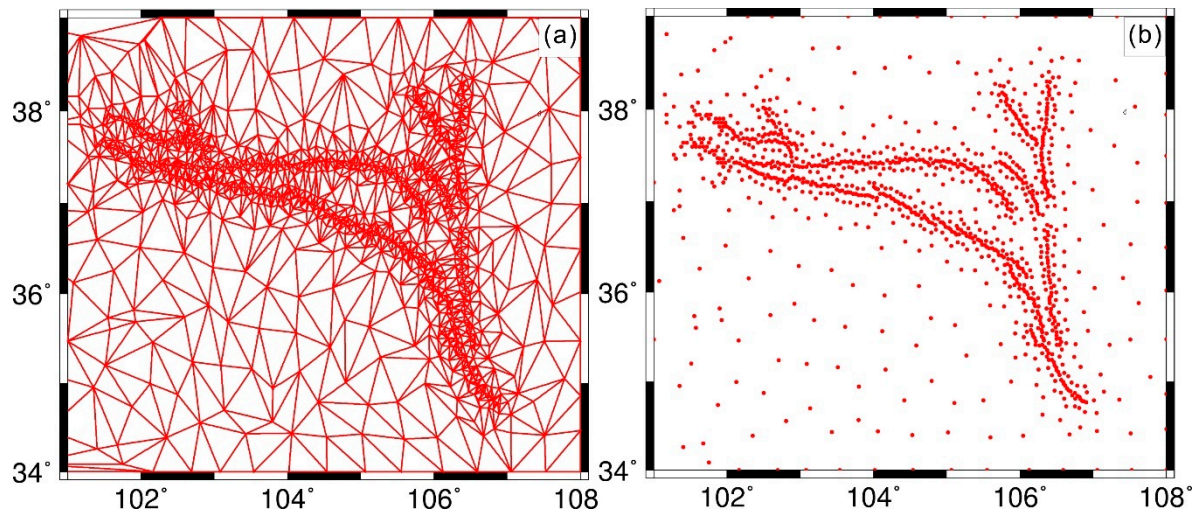


Figure S4. The results for the regional discretization. (a) An irregular grid for the Northeastern Tibetan area, meshed by using the free software DistMesh [49], with desired mesh density, i.e. dense points near the fault and sparse points far from the fault. (b) Discrete points from nodes of the mesh in (a), on which the horizontal velocities and strain rates are inverted from InSAR and GPS data.

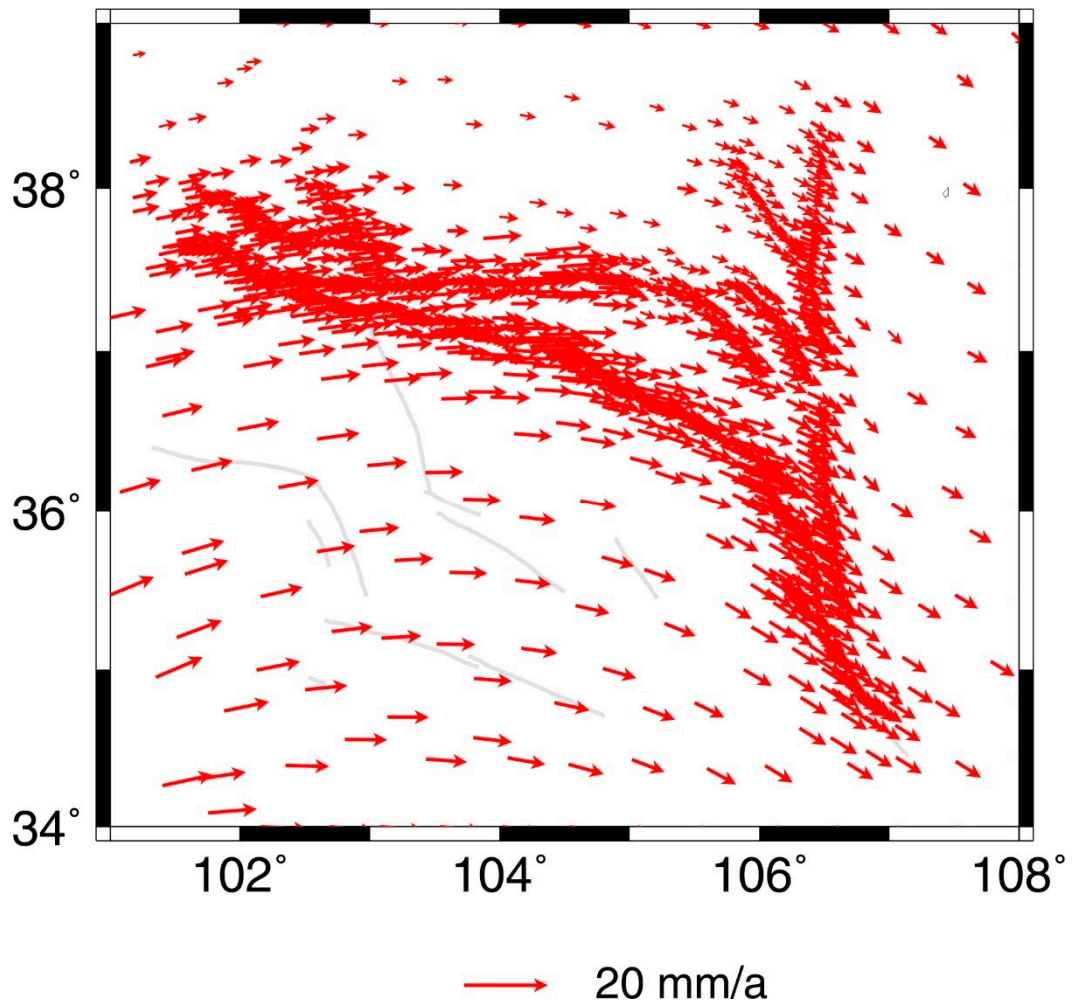


Figure S5. The fine horizontal velocity field inverted jointly by InSAR and GPS for the northeastern margin of the Tibetan Plateau.

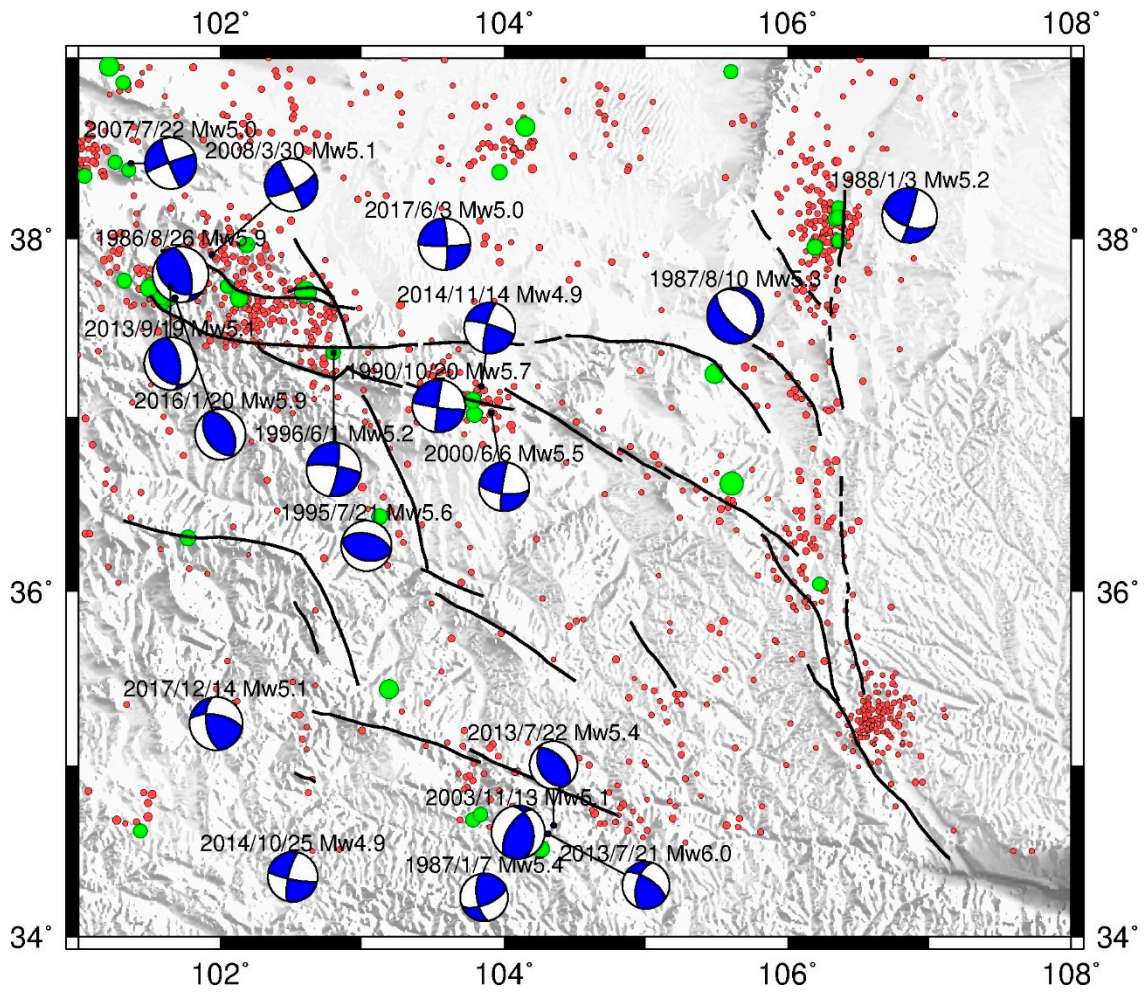


Figure S6. Regional seismicity map with 19 moderate earthquake since 1986. Green solid circles: the earthquakes with the magnitude more than 5.0. Red solid circles: the earthquakes with the magnitude less than 5.0.

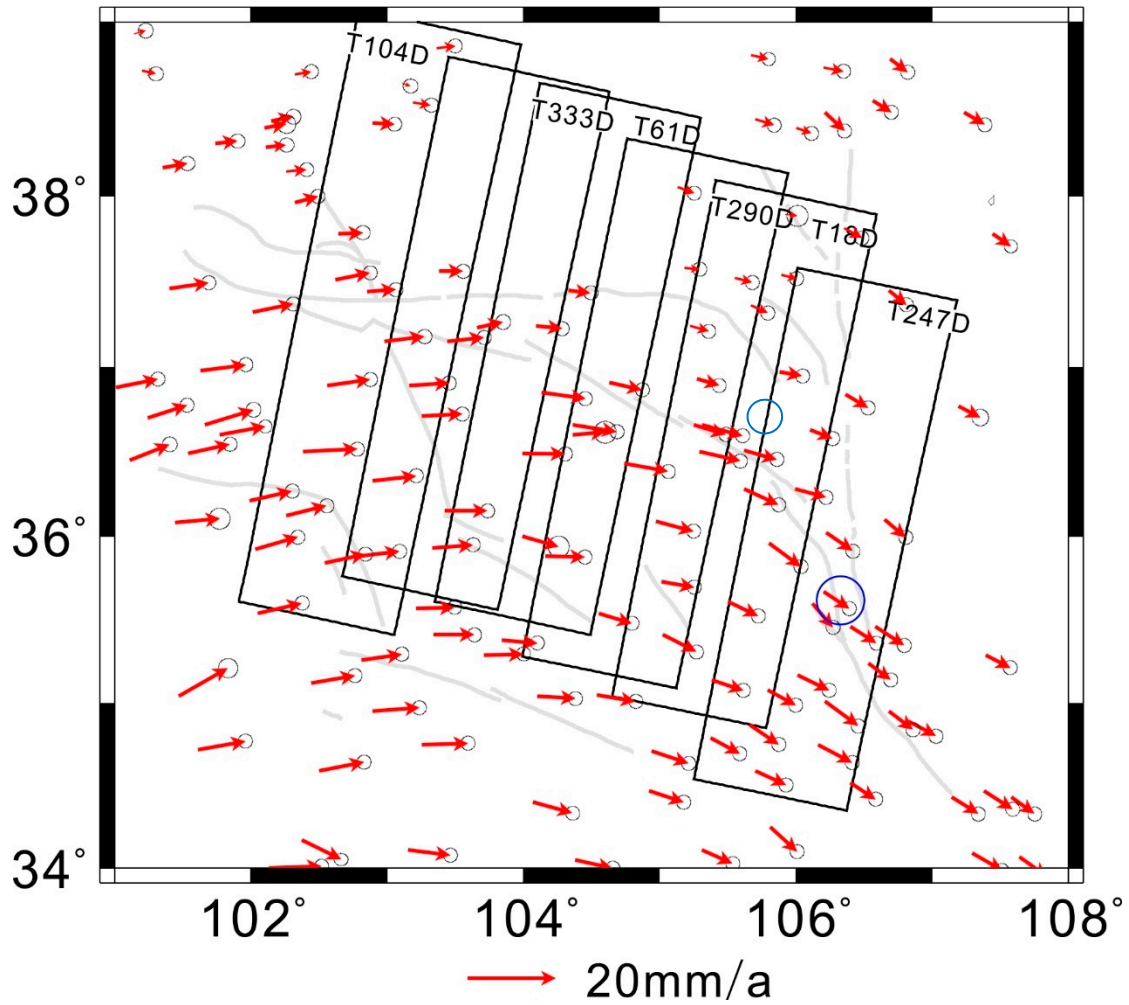


Figure S7. The GPS velocity field from Gan et al. [22] for the northeastern margin of the Tibetan Plateau. Near the Liupan Shan fault, one of GPS velocity denoted in blue circle in the west of the fault is small than the ones in the east, thus caused a tensional stress zone (see Figure 6c), which is contrary to the previous knowledge of squeezing structure. That is because local GPS observation dominates the inversion result in absence of high-coherenced InSAR data in this region.